

Role of Sterile Neutrino Warm Dark Matter in Rhenium and Tritium Beta Decays

H.J. de Vega

*LPTHE Université Pierre et Marie Curie (Paris VI),
Laboratoire Associé au CNRS UMR 7589, Tour 24, 5eme. étage,
Boite 126, Place Jussieu, 75252 Paris, cedex 05, France and
Observatoire de Paris, LERMA. Laboratoire Associé au CNRS UMR 8112.
61, Avenue de l'Observatoire, 75014 Paris, France.*

O. Moreno and E. Moya de Guerra

*Departamento de Física Atómica, Molecular y Nuclear,
Facultad de Ciencias Físicas, Universidad Complutense, 28040 Madrid, Spain*

M. Ramón Medrano

Departamento de Física Teórica I, Facultad de Ciencias Físicas, Universidad Complutense, 28040 Madrid, Spain

N. G. Sánchez

*Observatoire de Paris, LERMA. Laboratoire Associé au CNRS UMR 8112.
61, Avenue de l'Observatoire, 75014 Paris, France.*

(Dated: August 21, 2018)

Sterile neutrinos with mass in the range of one to a few keV are important as extensions of the Standard Model of particle physics and are serious dark matter (DM) candidates. This DM mass scale (warm DM) is in agreement with both cosmological and galactic observations. We study the role of a keV sterile neutrino through its mixing with a light active neutrino in Rhenium 187 and Tritium beta decays. We pinpoint the energy spectrum of the beta particle, $0 \lesssim T_e \lesssim (Q_\beta - m_s)$, as the region where a sterile neutrino could be detected and where its mass m_s could be measured. This energy region is at least 1 keV away from the region suitable to measure the mass of the light active neutrino, located near the endpoint Q_β . The emission of a keV sterile neutrino in a beta decay could show up as a small kink in the spectrum of the emitted beta particle. With this in view, we perform a careful calculation of the Rhenium and Tritium beta spectra and estimate the size of this perturbation by means of the dimensionless ratio \mathcal{R} of the sterile neutrino to the active neutrino contributions. We comment on the possibility of searching for sterile neutrino signatures in two experiments which are currently running at present, MARE and KATRIN, focused on the Rhenium 187 and Tritium beta decays respectively.

PACS numbers: 23.40.-s, 14.60.St, 14.60.Pq, 95.35.+d

Keywords: keV sterile neutrinos, beta decay, warm dark matter

I. INTRODUCTION

It is well known that dark matter (DM) is not described by the Standard Model (SM) of particle physics. Many extensions can be envisaged to include DM particles, coupled weakly enough to the SM particles to fulfill all particle experimental constraints, namely the fact that DM has not been detected so far in any particle physics experiment. On the other hand, cosmological and astrophysical constraints such as the ones coming from the dark matter density and the galaxy phase space density, or alternatively, the universal galaxy surface density, lead to DM candidates in the keV mass scale, namely warm DM (WDM), refs. [1–7]. A keV mass scale sterile neutrino is the front running candidate for WDM. Other possible WDM candidates in the keV mass scale are gravitinos, light neutralinos and majorons [1, 8].

Considering the first WDM candidate, sterile neutrinos can be naturally embedded in the SM of particle physics. They do not participate in weak interactions, and hence they are singlets of color, weak SU(2) and weak hypercharge. One sterile neutrino per lepton family could be expected, of which the lightest one (i.e. electron family) would have a lifetime of the order of the Hubble time and could be considered a DM candidate.

In this work, we consider the role played by a 1-2 keV sterile neutrino in Rhenium 187 and Tritium beta decay experiments. The left-handed neutrino flavor state ν_e (and equivalently for $\bar{\nu}_e$) will be a mixing of two mass eigenstates: one light active neutrino mass state (ν_l) and one keV scale sterile neutrino mass state (ν_s). Other neutrino mass states will not be taken into account for the time being. The mass m_l of the lightest active neutrino state is negligible ($m_l \ll \text{eV}$) in comparison with the mass m_s of the keV sterile mass state. The smallness of the mixing angle ζ makes sterile neutrinos difficult to detect.

Sterile neutrinos in the beta decay of Rhenium 187 are currently searched for by the Microcalorimeter Arrays for

a Rhenium Experiment (MARE) [9]. In this decay the available energy is $Q_\beta(^{187}\text{Re}) \simeq 2.469$ keV. The beta decay of Rhenium 187 into Osmium 187 is a first forbidden unique Gamow-Teller process ($5/2^+ \rightarrow 1/2^-$).

Up to now, the non observation of keV scale sterile neutrinos in the beta decay of Rhenium 187 gave an upper bound on the mixing angle $\zeta < 0.095$ for 1 keV steriles [10], which is compatible with the cosmological constraints on the mixing angle, $\zeta < 10^{-3}$, appropriate to produce enough sterile neutrinos to account for the observed DM. However, the amount of the sterile neutrinos that could be produced in the early universe also depends on the production mechanism, which is model dependent. We refer for that to the original references [3].

The Karlsruhe Tritium Neutrino Experiment (KATRIN) is currently studying the Tritium beta decay [13] and, if suitably adapted, it could study the presence of a sterile neutrino as well. In this decay the available energy is $Q_\beta(^3\text{H}_1) \simeq 18.6$ keV. The beta decay of Tritium into Helium 3 is an allowed transition ($1/2^+ \rightarrow 1/2^+$) with Fermi and Gamow-Teller contributions. Clearly, KATRIN has in principle the potential to detect sterile neutrinos with mass up to 18 keV. However, the main difficulty in detecting WDM sterile neutrinos comes from the smallness of the mixing angle between the active and sterile neutrino $\zeta < 10^{-3}$. Such range of values for ζ are too small for the present experimental sensitivities [13, 14] and would require a source with a large stability to reduce the systematic errors.

Detection of massive neutrinos by β -decay has been proposed in Ref. [15]. Other methods proposed to detect sterile neutrinos include measurements of the nuclear recoil [16, 17] and sterile neutrino capture on β -decaying nuclei [18].

In 1985 evidence for the emission of a 17 keV mass neutrino in Tritium beta decay was reported by J. J. Simpson [19]. The evidence was hotly debated, new experiments gave clear negative results and by 1993 the general conclusion was reached that there are no 17 keV neutrinos [20, 21]. The experiments in the nineties using ^{63}Ni , ^{35}S and other nuclei yielded an upper bound $\zeta < 0.03$ [20]. This bound is not restrictive for DM because the cosmological constraints based on the observed average DM density indicate for the currently popular models of DM sterile neutrinos a much lower bound, $\zeta < 10^{-3}$ [6, 7].

Sections II and III deal with keV dark matter from the cosmological and galactic point of view. WDM (DM particle mass between 1 keV and 10 keV, and decoupling temperature $T_d \sim 100$ GeV) produces the observed small (galactic) structures, as well as the large scale and cosmological structures, the observed cored density profiles and the right surface density value, while GeV WIMPS ($m \sim 100$ GeV, and $T_d \sim 5$ GeV, cold DM) inevitably produce a host of small-scale structures and cusped profiles which have not been observed, as well as a galaxy surface density much higher than observed. This summarizes our motivation for proposing a laboratory search for sterile neutrinos as DM candidates.

In Section IV we analyze the role that sterile neutrinos would play in the electron spectrum of Rhenium beta decay taking into account contributions from the electron s - and p -waves [11, 12]. The electron kinetic energy range T_e suitable for the detection of sterile neutrinos lies between 0 and $(Q_\beta - m_s)$, where m_s is the mass of the keV sterile neutrino. On the contrary, the electron kinetic energy region close to the endpoint energy Q_β is the one suitable for the detection of light active neutrinos. Systematic uncertainties such as Beta Environmental Fine Structure (BEFS) are not considered here [9]. In order to analyze the sterile neutrino effect, we introduce the dimensionless ratio \mathcal{R} of the sterile neutrino contribution to the active neutrino contribution. It allows us to compare two regions of the same spectrum: the one where the keV neutrino imprints a kink on the spectrum, and the one near the endpoint where the active light neutrino effect shows up. The Kurie function is also analyzed and expressed in terms of the ratio \mathcal{R} .

In Section V we study the role of sterile neutrinos in Tritium decay [13], where the emitted electrons are purely s -wave. Analogously to the Rhenium beta decay, the kinetic energy region relevant for the sterile neutrino detection is the low energy range $0 \leq T_e \leq (Q_\beta - m_s)$, while for the active neutrino it is the one close to the endpoint energy Q_β .

Finally, in Section VI we present our conclusions. Natural units $\hbar = c = 1$ are used all over this paper.

II. DARK MATTER

Although dark matter was noticed seventy-five years ago [22, 23], its nature is not yet known. Dark matter (DM) is needed to explain the observed structures in the Universe, in particular galaxies. DM particles must have been non-relativistic by the time of structure formation in order to reproduce the observed small structure at $\sim 2 - 3$ kpc.

The connection between the scale of the formed structure and the mass of the DM particle follows from the value of the free-streaming length l_{fs} [24]. This is the distance that the DM particles can freely travel. Structures at scales smaller than l_{fs} are erased by free-streaming and hence l_{fs} provides a lower bound on the size of DM dominated structures. WDM particles with mass in the keV scale give $l_{fs} \sim 100$ kpc while 100 GeV cold dark matter (CDM) particles produce an extremely small $l_{fs} \sim 0.1$ pc. A $l_{fs} \sim 100$ kpc is in nice agreement with the astronomical observations of galaxies [25] (smaller objects like stars are made up of baryons, not of DM), as well as at cosmological scales.

The GeV CDM free-streaming length l_{fs} is a million times smaller and would lead to the existence of a host of CDM smaller scale structures till the size of the solar system. No structure of such type has ever been observed. Lighter DM particles in the eV scale (hot dark matter, HDM) have a free-streaming length $l_{fs} \sim \text{Mpc}$ and hence would erase all existing structures below the Mpc scale in contradiction with all observations. This is why HDM has been ruled out [26].

The reason why CDM does not work is simple: CDM particles in the GeV scale are too slow (too cold), which prevents them to erase the small scale structure, while the eV particles (HDM) are excessively fast, which erases all structures. In between, WDM keV particles are able to produce the observed structures.

Astronomical observations strongly indicate that dark matter halos have cored profiles till scales below 1 kpc. On the contrary, CDM simulations (particles heavier than 1 GeV) always give cusped profiles. No cusped profiles have been ever observed. Linear profiles computed from the Boltzmann-Vlasov equation turn out to be cored for WDM and cusped for CDM indicating that WDM does reproduce the astronomical observations [5].

The surface density in DM-dominated galaxies is defined by $\mu_0 \equiv \rho_0 r_0$ where ρ_0 is the central core density and r_0 is the core radius. μ_0 turns out to be universal, taking the same value up to $\pm 10\%$ for galaxies of different sizes, morphologies, Hubble types and luminosities [27]. The surface density value predicted by CDM simulations is 1000 times larger than the observed value [28], while the surface density for keV WDM computed from the Boltzmann-Vlasov equation is in full agreement with the observed value of $120 (\text{MeV})^3$, indicating again that WDM does reproduce the astronomical observations [5].

Constraints of the DM particle mass to the keV range are obtained from combining theoretical analyses with the observed values of dark matter densities and phase space densities today (density over the cube of the velocity dispersion) of dwarf spheroidal galaxies.

Recent radioastronomy observations of velocity widths in galaxies from 21cm HI surveys clearly favours WDM over CDM [29]. WDM simulations contrasted to astronomical observations suggest a WDM particle mass slightly above 1 keV. Constraints from large scale structure give this value too [30]. Recent cosmological WDM N-body simulations with keV sterile neutrino WDM clearly show the agreement of the predicted small scale structures with the observations, while CDM simulations do not agree with observations at such scales [31].

None of the predictions of CDM simulations at small scales (cusps, substructures, dark disks, ...) have been observed. Here are some examples. The CDM satellite problem, namely that CDM simulations predict too many satellites in the Milky Way and only 1/3 of satellites predicted by CDM simulations around our galaxy are observed. The surface density problem, which consists of the galaxy surface density for CDM simulations being 1000 larger than observed [5, 28]. And the voids problem and the size problem, that have to do with the fact that CDM simulations do not produce big enough galaxies [32–34]. Further WDM properties are discussed in [35].

Notice that all DM observable effects discussed above only arise from the gravitational behaviour of the DM. Galaxy properties are independent of the non-gravitational couplings of the DM particles, provided that their couplings are small enough.

DM may decouple at or out of thermal equilibrium. The distribution function freezes out at decoupling. Whether they decouple at or out of equilibrium depends on the non-gravitational couplings of the DM particle. Normally, sterile neutrinos are so weakly coupled that they decouple out of thermal equilibrium. The functional form of the DM distribution function depends on the DM particle couplings and is therefore model dependent.

Sterile neutrinos can decay into an active-like neutrino and a monochromatic X-ray photon with an energy half the mass of the sterile neutrino. Observing the X-ray photon provides a way to observe sterile neutrinos in DM halos [36, 37].

WDM keV sterile neutrinos can be copiously produced in the supernovae cores. Supernovae (SN) stringently constrain the neutrino mixing angle squared to be $\lesssim 10^{-9}$ for $m > 100 \text{ keV}$, in order to avoid excessive energy lost. However, for smaller masses the SN bound is not so direct. Within the models worked out till now, mixing angles are essentially unconstrained by SN in the keV mass range [38].

Sterile neutrinos are produced out of thermal equilibrium and their production can be non-resonant, in the absence of lepton asymmetries, or resonantly enhanced, if lepton asymmetries are present. keV sterile neutrino WDM in minimal extensions of the Standard Model is consistent with Lyman-alpha constraints within a wide range of the model parameters. Lyman-alpha observations give a lower bound for the sterile neutrino mass of 4 keV only for sterile neutrinos produced in the case of a non-resonant (Dodelson-Widrow) mechanism [39, 40]. The Lyman-alpha lower bounds for the WDM particle mass are smaller in the Neutrino Minimal Standard Model, where sterile neutrinos are produced by the decay of a heavy neutral scalar, and for fermions in thermal equilibrium. Moreover, the number of observed Milky-Way satellites indicates lower bounds between 2 and 13 keV for different models of sterile neutrinos.

In summary, contrary to CDM, WDM essentially *works*, reproducing in a natural way the astronomical observations of structures over all scales, small as well as large and cosmological scales. The sterile neutrino with mass in the keV scale appears as a serious candidate for WDM. Galaxy observations alone cannot determine the DM particle properties other than the mass and the decoupling temperature. A direct particle detection is necessary to pinpoint and determine

which particle candidate describes DM. Beta decay is a promising way to detect DM sterile neutrinos.

III. DARK MATTER AND KEV STERILE NEUTRINOS

As it is known, DM is not described by the Standard Model (SM) of particle physics. However, many extensions of the SM can be envisaged to include a DM particle with mass in the keV scale and coupled weakly enough to the Standard Model particles so as to fulfill all particle physics experimental constraints, coming mainly from the fact that DM has not been detected so far in any particle physics experiment. Besides sterile neutrinos, possible DM candidates in the keV mass scale are gravitinos, light neutralinos, majorons, etc. [8].

As particle physics motivations for sterile neutrinos one can advance that there are both left- and right-handed quarks (with respect to chirality) while active neutrinos are only left-handed. It is thus natural to have right-handed neutrinos ν_R besides the known left-handed active neutrinos. This argument is called ‘quark-lepton similarity’.

Sterile neutrinos can be naturally embedded in the SM of particle physics with the symmetry group $SU(3)_{color} \otimes SU(2)_{weak} \otimes U(1)_{weak\ hypercharge}$. Leptons are singlets under color SU(3) and doublets under weak SU(2) in the SM. Sterile neutrinos ν_R do not participate in weak interactions. Hence, they must be singlets of color SU(3), weak SU(2) and weak hypercharge U(1).

Let us consider a simple embedding of the sterile neutrino in the Standard Model. More elaborated sterile neutrino models have been put forward [43]. The SM Higgs Φ is a SU(2) doublet with a nonzero vacuum expectation value Φ_0 . This allows a Yukawa-type coupling with the left- and right-handed leptons:

$$L_{Yuk} = y \bar{\nu}_L \nu_R \Phi_0 + h.c. , \quad (1)$$

where y is the Yukawa coupling, and

$$\Phi_0 = \begin{pmatrix} 0 \\ v \end{pmatrix} , \quad v = 174 \text{ GeV}. \quad (2)$$

These terms in the Lagrangian induce a mixing (bilinear) term between ν_L and ν_R allowing for transmutations $\nu_L \Leftrightarrow \nu_R$. Mixing and oscillations of particle states are typical of low energy particle physics. Further well known examples are: (i) flavor mixing: e - μ neutrino oscillations, which explain solar neutrinos, (ii) $K^0 - \bar{K}^0$, $B^0 - \bar{B}^0$ and $D^0 - \bar{D}^0$ meson oscillations in connection with CP-violation.

As a consequence of the Lagrangian in Eq. (1), the neutrino mass matrix takes the form

$$(\bar{\nu}_L \bar{\nu}_R) \begin{pmatrix} 0 & m_D \\ m_D & M \end{pmatrix} \begin{pmatrix} \nu_L \\ \nu_R \end{pmatrix} \quad (3)$$

where M is the mass term of the right-handed neutrino ν_R , and $m_D = y v$ with $M \gg m_D$.

The masses of the active and sterile neutrinos are given by the seesaw mechanism. The mass eigenvalues in this simple model take the form: m_D^2/M (active neutrino) and M (sterile neutrino), with eigenvectors $\nu_{active} \simeq \nu_L - \frac{m_D}{M} \nu_R$ (active neutrino) and $\nu_{sterile} \simeq \nu_R + \frac{m_D}{M} \nu_L$, $M \gg m_D^2/M$ (sterile neutrino). Choosing $M \sim 1$ keV and $m_D \sim 0.1$ eV yields m_D^2/M about 10^{-5} eV, consistent with observations. This corresponds to a mixing angle $\zeta \sim m_D/M$ about 10^{-4} and would be appropriate to produce enough sterile neutrinos to account for the observed DM. However, notice that the amount of the sterile neutrinos produced in the early universe also depends on the production mechanism, which is model dependent. The smallness of the mixing angle ζ makes sterile neutrinos difficult to detect.

One sterile neutrino per lepton family could be expected, of which the lightest one (i.e. electron family) would have a lifetime of the order of the Hubble time and could be considered a DM candidate. In summary, the empty slot of right-handed neutrinos in the Standard Model of particle physics could be filled in a fully consistent way by keV-scale sterile neutrinos describing the DM.

IV. RHENIUM 187 BETA DECAY AND STERILE NEUTRINO MASS

As a probe to detect possible mixing of keV sterile neutrinos with light active neutrinos, we consider in this section the beta decay of Rhenium 187 (^{187}Re ; $Z = 75$, $A = 187$) into Osmium 187 (^{187}Os ; $Z = 76$, $A = 187$),

$$^{187}\text{Re} \rightarrow ^{187}\text{Os} + e^- + \bar{\nu}_e \quad (4)$$

The neutrino flavor eigenstate ν_e (and equivalently for $\bar{\nu}_e$) can be written as a combination of light active (subscript i) and heavy sterile mass eigenstates as [6, 15]

$$|\nu_e\rangle = \sum_i U_{ei} |\nu_i\rangle + \sum_s U_{es} |\nu_s\rangle \quad (5)$$

where the quantities U belong to the unitary leptonic mixing matrix. For the purpose of this paper, we approximate this combination as a mixing of two mass eigenstates given by [6]

$$|\nu_e\rangle = \cos\zeta |\nu_l\rangle + \sin\zeta |\nu_s\rangle \quad (6)$$

where ζ is the mixing angle between a light neutrino mass state ν_l , and the heavy sterile neutrino mass state ν_s . Other neutrino mass states will not be taken into account in this work. An effective mass m_l can be used for the former combination of light mass active neutrinos, but its value ($m_l \lesssim \text{eV}$) is negligible in comparison with the sterile neutrino mass in the keV scale. As for the mixing angle ζ , the cosmological constraints based on the observed average DM density suggest [6, 7]

$$\sin^2\zeta \sim 10^{-8} \quad , \quad \zeta \sim 0.006^\circ \quad . \quad (7)$$

We should keep in mind that these constraints on the value of ζ depend both on the sterile neutrino model and on the sterile neutrino production mechanism. Eq. (7) corresponds to currently popular models of DM sterile neutrino [6, 7].

^{187}Re is a long half-life isotope ($t_{1/2} \simeq 4.35 \cdot 10^{10}$ years), with ground state spin-parity assignment $J^\pi = 5/2^+$, that has a single β^- -decay branch mode to the ground state $1/2^-$ of ^{187}Os with an endpoint energy $Q_\beta \simeq 2.469$ keV ($Q_\beta = T_e + m_\nu + T_\nu$, where T_e and T_ν are kinetic energies of the electron and the neutrino respectively).

In this transition, the change of total angular momentum is $\Delta J = 2$ and there is also a change of parity ($\Delta\pi = -$). Therefore we are dealing at best with a first forbidden Gamow-Teller process. The lepton system ($e - \bar{\nu}$) carries an orbital angular momentum $L = 1$ (first forbidden transition) and a spin $S = 1$ (unique Gamow-Teller transition), that couple to the total angular momentum $J = 2$. The two possible angular momentum components of the system, $[(l_j)_e(l_j)_{\bar{\nu}}]_{J=2}$, are $[(p_{3/2})_e(s_{1/2})_{\bar{\nu}}]_{J=2}$ and $[(s_{1/2})_e(p_{3/2})_{\bar{\nu}}]_{J=2}$. Therefore, as noted in [11], the total differential decay rate $d\Gamma/dE_e$ is a sum of the two contributions corresponding to the emission of electrons in p -wave and in s -wave

$$\frac{d\Gamma}{dE_e} = \frac{d\Gamma_{p_{3/2}}}{dE_e} + \frac{d\Gamma_{s_{1/2}}}{dE_e} \quad (8)$$

Following Eq. (6), we write the theoretical spectral shape of the electron in an (l_j) -wave as a sum of the contributions from light (l) and sterile (s) neutrinos,

$$\frac{d\Gamma_{l_j}}{dE_e} = \frac{d\Gamma_{l_j}^l}{dE_e} \cos^2\zeta + \frac{d\Gamma_{l_j}^s}{dE_e} \sin^2\zeta \quad (9)$$

where

$$\frac{d\Gamma_{l_j}^\chi}{dE_e} = C B_{Re} R_{Re}^2 p_e p_{\nu_\chi} E_e (E_0 - E_e) F_0(Z, E_e) S_l(p_e, p_{\nu_\chi}) \theta(E_0 - E_e - m_\chi) \quad , \quad (10)$$

for $\chi = l, s$. Z stands for the atomic number of the daughter nucleus, $F_0(Z, E_e)$ is the Fermi function and $\theta(E_0 - E_e - m_\chi)$ is the step function. R_{Re} is the nuclear radius [44], B_{Re} is the dimensionless squared nuclear reduced matrix element (r.m.e.) and C is a constant to be defined later on. In the above expression, E_e , E_0 and $p_e = \sqrt{E_e^2 - m_e^2}$ are the total energy, maximum total energy and momentum of the emitted electron respectively, and $p_\nu = \sqrt{(E_0 - E_e)^2 - m_\nu^2}$ is the momentum of the emitted neutrino.

Being Q_β the endpoint energy, we have $E_0 = m_e + Q_\beta$, and the kinematical ranges of E_e , p_e and p_ν for zero neutrino mass are as follows

$$m_e \leq E_e \leq m_e + Q_\beta; \quad 0 \leq p_e \leq \sqrt{Q_\beta^2 + 2m_e Q_\beta}; \quad 0 \leq p_\nu \leq Q_\beta. \quad (11)$$

The shape factor $S_l(p_e, p_\nu)$ appears in forbidden decays. For the case of interest here, a first forbidden decay, l takes the value $l = 0$ for the s -wave and $l = 1$ for the p -wave electrons, with shape factors

$$S_0(p_e, p_\nu) = \frac{1}{3} p_\nu^2 \quad \text{and} \quad S_1(p_e, p_\nu) = \frac{1}{3} p_e^2 \frac{F_1(Z, E_e)}{F_0(Z, E_e)}. \quad (12)$$

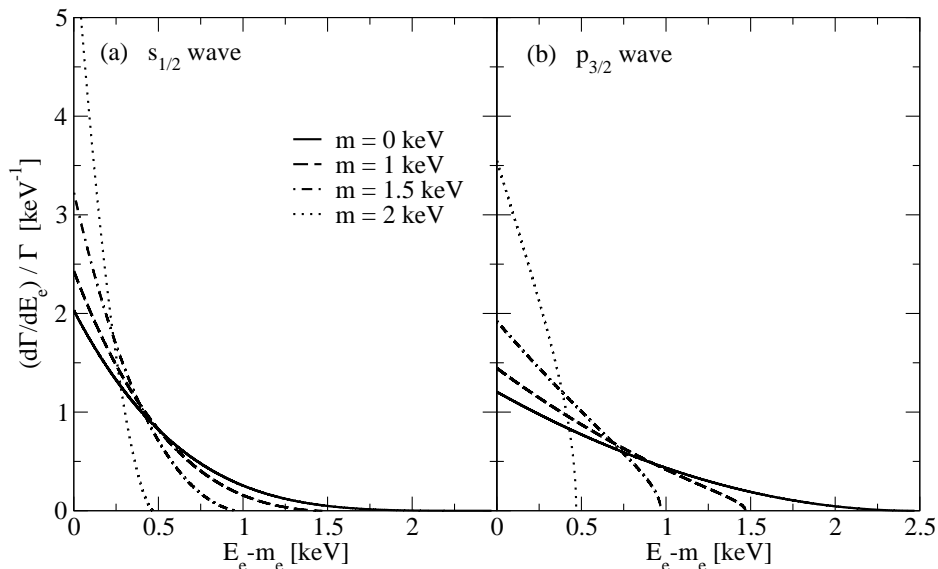


FIG. 1: Contributions of s -wave (left) and p -wave (right) electrons to the normalized differential decay rate of the process ^{187}Re to ^{187}Os plotted against the electron kinetic energy $E_e - m_e$. Selected values of the sterile neutrino mass are used, $m_s = 1, 1.5, 2$ keV (dashed, dashed-dotted and dotted lines, respectively), compared to the light neutrino case $m_l = 0$ (solid line).

The relativistic Fermi functions $F_0(Z, E_e)$ and $F_1(Z, E_e)$ account for the Coulomb interaction between the residual nucleus ($Z = 76$ in our case) and the emitted electron in the s and p -waves respectively. They are defined as

$$F_{k-1} = \left[\frac{\Gamma(2k+1)}{\Gamma(k)\Gamma(1+2\gamma_k)} \right]^2 (2p_e R)^{2(\gamma_k-k)} |\Gamma(\gamma_k + iz)|^2 e^{\pi z} \quad (13)$$

and depend on the strength of the Coulomb interaction, given by the fine structure constant $\alpha \simeq 1/137.03$, through

$$\gamma_k = \sqrt{k^2 - (\alpha Z)^2} \quad \text{and} \quad z = \alpha Z \frac{E_e}{p_e}, \quad (14)$$

$k = 1, 2$ in our case. We note that the Fermi functions in Eq. (13) satisfy $F_{k-1}(Z \rightarrow 0, E_e) \rightarrow 1$ for $\alpha Z \rightarrow 0$ and for any $k \geq 1$. The constant factor C in Eq. (10) is given by

$$C \equiv \frac{G_F^2 V_{ud}^2 c_V^2}{2\pi^3} \simeq 2 \times 10^{-36} (\text{keV})^{-4}, \quad (15)$$

where G_F is the Fermi constant, V_{ud} the element of the Cabibbo-Kobayashi-Maskawa matrix ($|V_{ud}| \simeq 0.97$), and $c_V \simeq 1$ is the strength of the vector charged weak interaction. The dimensionless squared nuclear reduced matrix element (r.m.e.), B_{Re} , can be computed directly from the experimental ^{187}Re mean-life $\tau = t_{1/2}/\ln 2$ as [see Eq. (10)]

$$B_{Re}^{-1} = \tau C R_{Re}^2 \int_{m_e}^{E_0} p_e p_\nu E_e (E_0 - E_e) F_0(Z, E_e) S(p_e, p_\nu) dE_e, \quad (16)$$

and it takes the value $B_{Re} \simeq 3.6 \times 10^{-4}$ for a value of the nuclear radius R_{Re} approximated as $R_{Re} \simeq 1.2 \times (187)^{1/3} \text{fm} \simeq 6.86 \text{fm}$. Microscopic calculations of these quantities are in progress.

In Fig. 1 we represent the s -wave (left) decay rates, $d\Gamma_{s_{1/2}}^l/dE_e$ and $d\Gamma_{s_{1/2}}^s/dE_e$, and the p -wave (right) decay rates $d\Gamma_{p_{3/2}}^l/dE_e$ and $d\Gamma_{p_{3/2}}^s/dE_e$, normalized to one. We plot the sterile neutrino contribution for s and p -wave outgoing electrons and for selected values of the sterile neutrino mass, $m = 1, 1.5$ and 2 keV (dashed, dash-dotted and dotted line respectively), compared to the light neutrino case with $m = 0$ (solid line).

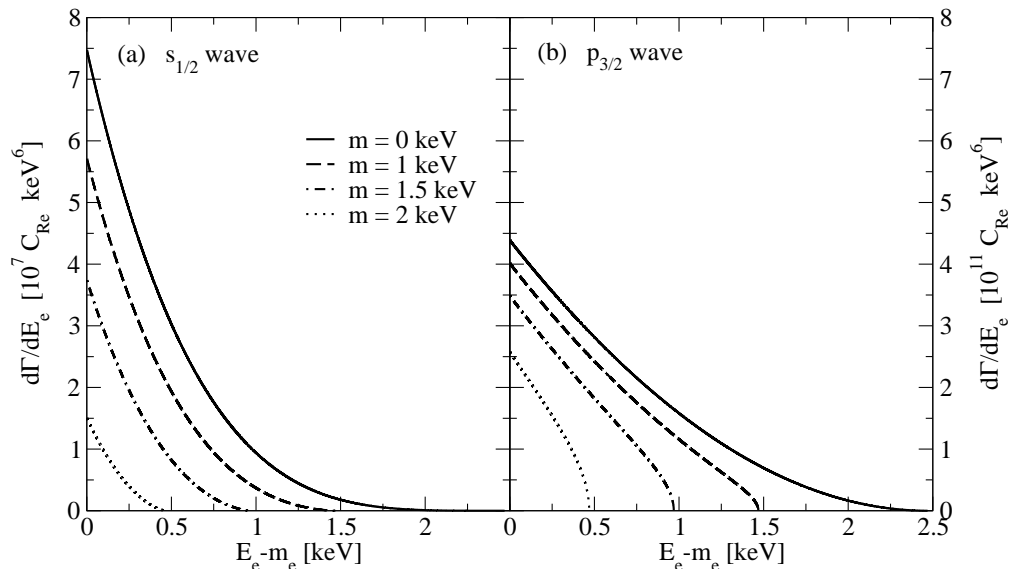


FIG. 2: Contributions of s -wave (left) and p -wave (right) electrons to the process ^{187}Re to ^{187}Os as in Fig. 1 but for unnormalized decay rates, in units of $10^7 C_{Re} \text{ keV}^6$ (left) and of $10^{11} C_{Re} \text{ keV}^6$ (right). The maximum differential decay rate for s -wave electrons is of the order of 10^7 , whereas for p -wave electrons it is 10^{11} . The p -wave dominates by four orders of magnitude for both light and sterile neutrino emission and so the spectral shape of beta decay is dictated by the r.h.s. panel.

In Fig. 2, we represent the unnormalized decay rates, on the left $d\Gamma_{s_{1/2}}^l/dE_e$ and $d\Gamma_{s_{1/2}}^s/dE_e$, and on the right $d\Gamma_{p_{3/2}}^l/dE_e$ and $d\Gamma_{p_{3/2}}^s/dE_e$. The same choices of neutrino masses as in Fig. 1 are considered. As seen in the plots, the maximum differential decay rate for s -wave electrons is of the order of 10^7 whereas for p -wave electrons it is 10^{11} (in units of $C_{Re} \text{ keV}^6 \equiv C B_{Re} R_{Re}^2 \text{ keV}^6$). This dominance by four orders of magnitude of the p -wave that was noticed both theoretically [11] and experimentally [12] for the light neutrino emission, holds also for sterile neutrino emission. This is why the spectral shape of beta decay is dictated by the curves shown in the r.h.s. panel of Fig. 2.

The effect of the sterile neutrino emission on the electron spectral shape is represented in Fig. 3 by comparing the differential decay rate $d\Gamma/dE_e$ for $m = 1 \text{ keV}$ with (solid line) and without (dashed line) neutrino contribution for $\zeta = 0.01^\circ$. The two curves start to deviate at the step point $T_e = Q_\beta - m_s = 1.469 \text{ keV}$, where the sterile neutrino starts to contribute, and the difference grows as T_e goes to zero. The region where the kink appears is shown in the inset on a magnified scale as a function of $E_e - m_e - Q_\beta + m_s$ in eV. The chosen value of the mixing angle (0.01°) is inspired on Fig. 8 in Ref. [37], where a plot is made of upper bounds for the mixing angle as a function of the sterile neutrino mass based on X-ray observations of dwarf spheroidal galaxies. For different values of the mixing angle the effect scales as the function \mathcal{R} that we define below.

In order to analyze the possible effect of a sterile neutrino, we introduce the dimensionless function

$$\mathcal{R} \equiv \frac{d\Gamma^s/dE_e}{d\Gamma^l/dE_e} \tan^2 \zeta \quad (17)$$

which is the ratio between the sterile and light neutrino contributions to the total decay rate times the tangent square of the mixing angle. The function \mathcal{R} is largest for p_e (or T_e) going to zero. This procedure is useful because we are comparing two regions of the same spectrum: the region where $(E_e - m_e) < (Q_\beta - m_s)$ and the emitted neutrino has enough energy for the sterile neutrino ($m_s \sim \text{keV}$) to imprint an effect on the spectrum, and the region where $(E_e - m_e) > (Q_\beta - m_s)$ and the sterile neutrino effect does not show up. Clearly, there is a *step* in the spectrum for $E_e - m_e = Q_\beta - m_s$ which could be observed if the experimental relative error in this energy region is lower than the height of the step.

The ratio \mathcal{R} , Eq. (17), is shown in Fig. 4 as a function of the electron momentum p_e for a mixing angle $\zeta = 0.01^\circ$, and for different values of the neutrino masses, $m_s = 0, 1, 1.5$ and 2 keV , corresponding to the solid, dashed, dash-dotted and dotted lines respectively. As can be seen in this figure, the ratio is different from zero in the range

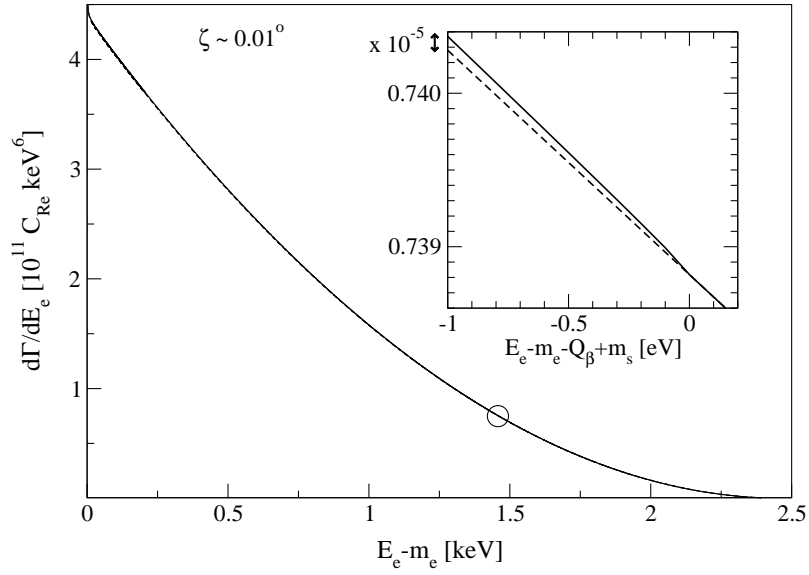


FIG. 3: The ^{187}Re to ^{187}Os beta particle spectrum in units of $10^{11} C_{Re} \text{ keV}^6$, for a mixing angle $\zeta = 0.01^\circ$ and sterile mass $m_s = 1 \text{ keV}$. The curves with (solid) and without (dashed) sterile neutrino contribution are indistinguishable in the main plot, but are shown in the inset as a function of $E_e - m_e - Q_\beta + m_s$ in eV, with a separation between them magnified as indicated.

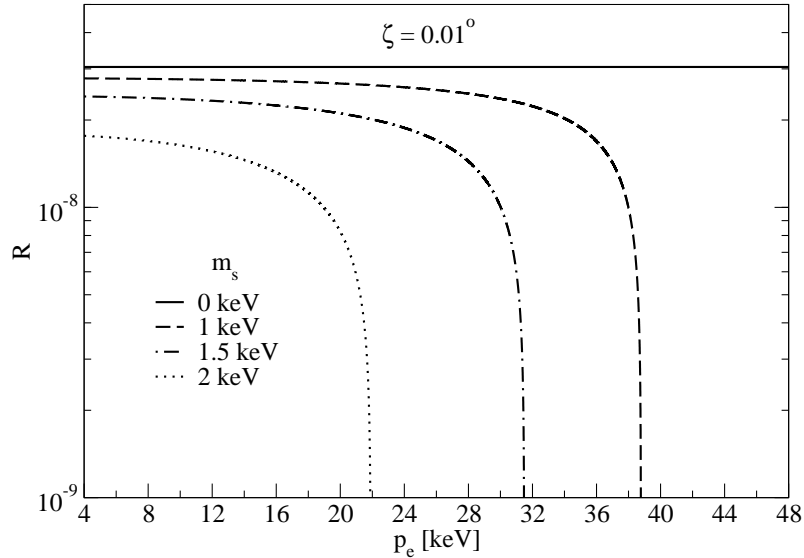


FIG. 4: Ratio \mathcal{R} , Eq. (17), of the sterile neutrino to the active neutrino contributions of the process ^{187}Re to ^{187}Os vs. the electron momentum for a fixed mixing angle $\zeta = 0.01^\circ$ and different sterile neutrino masses, $m_s = 0, 1, 1.5$ and 2 keV (solid, dashed, dashed-dotted and dotted lines, respectively). \mathcal{R} increases with decreasing m_s . \mathcal{R} is nonzero in a range $0 < p_e < p_{max}$ and p_{max} decreases as m_s increases.

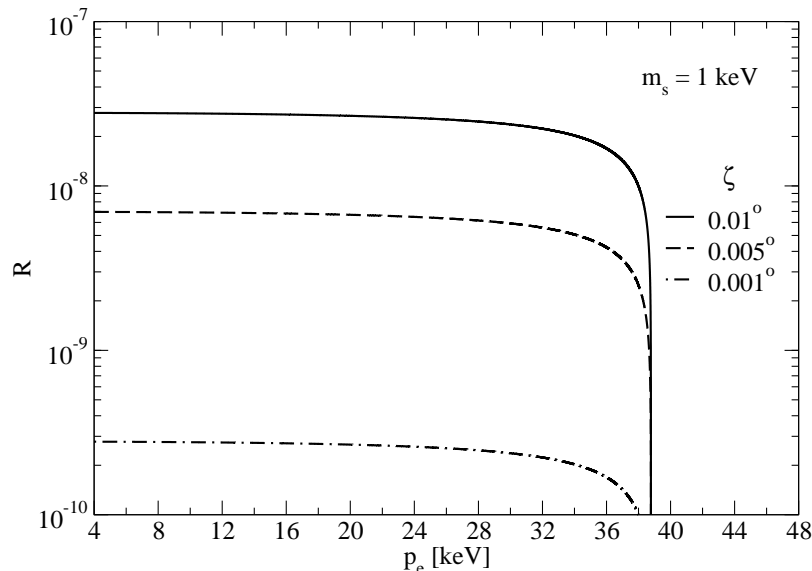


FIG. 5: The ratio \mathcal{R} as in Fig. 4 but for a fixed sterile neutrino mass $m_s = 1$ keV and different mixing angles, $\zeta = 0.01^\circ$, 0.005° , 0.001° (solid, dashed, dashed-dotted lines, respectively) of the process ^{187}Re to ^{187}Os . \mathcal{R} is almost constant in the range $0 < p_e < p_{max}$ and increases with ζ .

$0 \leq p_e < (p_e)_{max}$, with $(p_e)_{max} = [(Q_\beta - m_s)(Q_\beta - m_s + 2m_e)]^{1/2}$. For example, for $m_s = 2$ keV, $(p_e)_{max} \simeq 21.9$ keV, and for $m_s = 1$ keV, $(p_e)_{max} \simeq 38.8$ keV. Notice that when m_s increases, \mathcal{R} decreases.

Similarly, in Fig. 5 we show the ratio \mathcal{R} as a function of the electron momentum p_e but for a fixed sterile neutrino mass of $m_s = 1$ keV and different light-sterile mixing angles $\zeta = 0.01^\circ$, 0.005° , 0.001° . Figure 5 shows not only the increase of \mathcal{R} with increasing mixing angle for a fixed value of m_s , but also shows the fact that for fixed values of m_s and ζ , the ratio \mathcal{R} is almost constant in the region $0 < p_e < (p_e)_{max}$.

From Eq. (8) and Eq. (9), we write

$$\frac{d\Gamma}{dE_e} = \frac{d\Gamma^l}{dE_e} [1 + \mathcal{R}] \cos^2 \zeta, \quad (18)$$

where $d\Gamma/dE_e$ is the total differential decay rate when neutrino mixing is present ($\zeta \neq 0$), and $d\Gamma^l/dE_e$ is the differential decay rate for the light neutrino (no mixing: $\zeta = 0$). For small mixing angle ζ , the differential decay rate $d\Gamma/dE_e$ [Eq. (18)] normalized to $d\Gamma^l/dE_e$ is

$$\frac{d\Gamma/dE_e}{d\Gamma^l/dE_e} \simeq 1 + \mathcal{R}, \quad (19)$$

which shows that for small mixing angle the ratio between the differential decay rates with mixing and without mixing is given by $1 + \mathcal{R}$. This ratio is larger for p_e or T_e going to zero.

We want to emphasize that the energy region suitable for creation and detection of the keV sterile neutrino corresponds to low p_e or T_e . On the contrary, information on active neutrinos should be obtained from the region of T_e close to the endpoint energy Q_β .

From eqs. (8), (10) and (12), we can write for the function \mathcal{R} the explicit expression

$$\mathcal{R} = \frac{p_{\nu_s}^3}{p_{\nu_l}^3} \theta(Q_\beta - T_e - m_s) \frac{1 + \frac{p_e^2}{p_{\nu_s}^2} \frac{F_1(Z, E_e)}{F_0(Z, E_e)}}{1 + \frac{p_e^2}{p_{\nu_l}^2} \frac{F_1(Z, E_e)}{F_0(Z, E_e)}} \tan^2 \zeta \quad (20)$$

In order to analyze the ratio $p_e^2 F_1(Z, E_e)/F_0(Z, E_e)$, it is worth to define $F_{k-1}(Z, E_e)$ as

$$F_{k-1}(Z, E_e) \equiv C_{k-1} d_{k-1} \left(\frac{m_e}{p_e}\right)^{2k-1} \left(\frac{E_e}{m_e} \alpha Z\right)^{2\gamma_{k-1}} \quad (21)$$

where

$$C_{k-1} \equiv 2\pi (2m_e R)^{2(\gamma_{k-1}-k)} \left[\frac{\Gamma(2k+1)}{\Gamma(k)\Gamma(1+2\gamma_k)}\right]^2 ; \quad d_{k-1} \equiv \frac{1}{2\pi} \left(\frac{E_e}{p_e} \alpha Z\right)^{1-2\gamma_k} \left|\Gamma\left(\gamma_k + i \alpha Z \frac{E_e}{p_e}\right)\right|^2 e^{\pi \alpha Z \frac{E_e}{p_e}} \quad (22)$$

γ_k is defined by Eq. (14) and $d_{k-1}(\alpha Z E_e/p_e) \rightarrow 1$ for $p_e \rightarrow 0$ (for all k). The above definitions yield again $F_{k-1} \rightarrow 1$ for $\alpha Z \rightarrow 0$ (for all k). In this respect, eqs. (21) and (22) differ from references [11] and [41, 42]. Finally, the ratio in the shape factor of Eq.(12) for $l = 1$ is given by

$$\frac{p_e^2 F_1(Z, E_e)}{F_0(Z, E_e)} = \frac{C_1}{C_0} \frac{d_1}{d_0} m_e^2 \left(\frac{E_e}{m_e} \alpha Z\right)^{2(\gamma_2-\gamma_1)} \quad (23)$$

and for $p_e \rightarrow 0$

$$\frac{p_e^2 F_1(Z, E_e)}{F_0(Z, E_e)} \underset{p_e \rightarrow 0}{\sim} 0.14 m_e^2, \quad (24)$$

[$d_1/d_0 \rightarrow 1$ for $p_e \rightarrow 0$].

From Eq. (20) and Eq. (24), we have

$$\mathcal{R} \underset{p_e \rightarrow 0}{\sim} \frac{p_{\nu_s}}{p_{\nu_l}} \tan^2 \zeta. \quad (25)$$

For $p_e \rightarrow 0$ the maximum neutrino momenta are: $(p_{\nu_s})_{\max} \sim 1.45$ keV, 2.26 keV for $m_s \simeq 2$ keV, 1 keV respectively; and $(p_{\nu_l})_{\max} = 2.469$ keV for $m_l = 0$ keV.

We have shown the relevance of the function \mathcal{R} to the analysis of the sterile neutrino effect. One can also study the effect of a sterile neutrino through the difference between the decay rate with mixing ($\zeta \neq 0$) and the reference case without mixing ($\zeta = 0$). This difference is very small, since the mixing is in any case small, as it is expressed in the following ratio,

$$\mathcal{R}^* = \frac{\left[\frac{d\Gamma}{dE_e}\right]_{\zeta \neq 0} - \left[\frac{d\Gamma}{dE_e}\right]_{\zeta=0}}{\left[\frac{d\Gamma}{dE_e}\right]_{\zeta=0}} = \left(-1 + \frac{d\Gamma^s/dE_e}{d\Gamma^l/dE_e}\right) \sin^2 \zeta = \frac{d\Gamma/dE_e}{d\Gamma_l/dE_e} - 1, \quad (26)$$

which can be written as well as a function of \mathcal{R}

$$\mathcal{R}^* = -\sin^2 \zeta + \mathcal{R} \cos^2 \zeta \quad (27)$$

In Fig. 6 we plot the quantity \mathcal{R}^* for a fixed sterile mass $m_s = 1$ keV and for different mixing angles. The Kurie function is defined as

$$K(y) = \sqrt{\frac{d\Gamma/dE_e}{p_e E_e F_0(Z, E_e) S_1(Z, E_e)}} \quad , \quad y \equiv E_0 - E_e = Q - T_e \geq 0 \quad . \quad (28)$$

Considering the mixing between the light and sterile neutrinos, $K(y)$ can be written as

$$K(y) = \sqrt{K_l^2(y) \cos^2 \zeta + K_s^2(y) \sin^2 \zeta} \quad (29)$$

where

$$K_\chi(y) = \sqrt{\frac{d\Gamma^\chi/dE_e}{p_e E_e F_0(Z, E_e) S_1(Z, E_e)}} \quad , \quad \chi = l, s \quad . \quad (30)$$

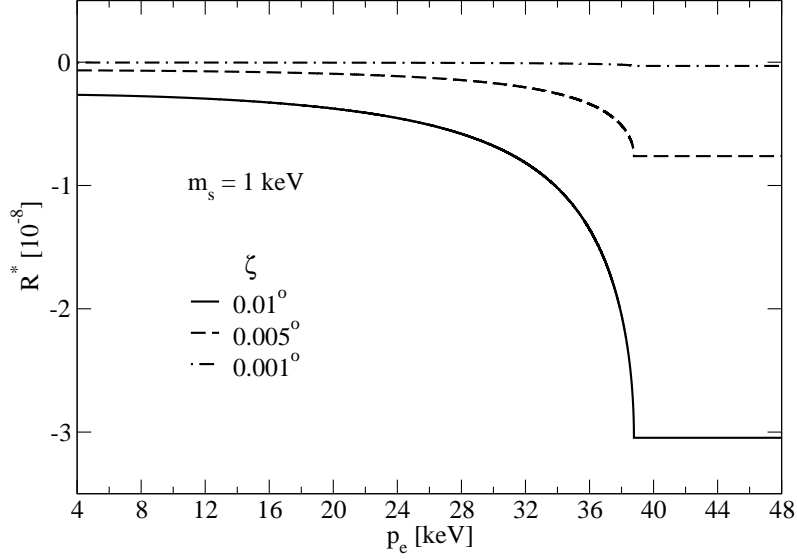


FIG. 6: Same as in Fig. 5 but for \mathcal{R}^* , Eq. (26 or Eq. (27), in units of 10^{-8} for fixed m_s and different mixing angles of the process ^{187}Re to ^{187}Os . The small p_e region is always the best for the sterile neutrino detection.

For $\zeta = 0$ (no sterile-light neutrino mixing), and due to the introduction of $F_0(Z, E_e) S_1(Z, E_e)$ in the denominator, $K(y)$ vs. y is a straight line for $m_l \simeq 0$. This follows straightforwardly from Eq. (28) for $K(y)$ and from Eq. (10) for $d\Gamma/dE_e$, setting $m_l = 0$ and $p_\nu = E_0 - E_e = y$, and it therefore follows that $K(y) \simeq \text{const} \times y$. $K(y)$ can be written as well in terms of \mathcal{R} Eq. (17),

$$K(y) = K_l(y) \sqrt{1 + \mathcal{R}} \cos \zeta. \quad (31)$$

Finally, in Fig. 7 we present the Kurie plot K considering several neutrino masses, and K_l (solid line).

V. TRITIUM BETA DECAY AND STERILE NEUTRINO MASS

Let us now consider the beta decay of Tritium (^3H ; $Z = 1$; $A = 3$)



as a probe to detect a possible mixing of keV sterile neutrinos with active neutrinos. Tritium beta decay would allow the detection of sterile neutrinos heavier than in the Rhenium beta decay case, within the 1 to 10 keV range suggested by cosmological and galactic observations. Tritium, ^3H , is a hydrogen isotope going to the helium isotope ^3He , with a half-life $t_{1/2} \simeq 12.33$ years, endpoint energy $Q_\beta \simeq 18.59$ keV, and a spin-parity transition $1/2^+ \rightarrow 1/2^+$.

For the Tritium decay case there is no change in angular momentum and parity corresponding to an allowed transition ($L = 0$) with Fermi ($S = 0$) and Gamow-Teller ($S = 1$) components. Therefore, the electron is emitted in s -wave and the differential decay rate is simply

$$\frac{d\Gamma}{dE_e} = \frac{d\Gamma_{s_{1/2}}}{dE_e} \quad (33)$$

Similarly to Eq. (9) and Eq. (10) we have

$$\frac{d\Gamma_{s_{1/2}}}{dE_e} = \frac{d\Gamma_{s_{1/2}}^l}{dE_e} \cos^2 \zeta + \frac{d\Gamma_{s_{1/2}}^s}{dE_e} \sin^2 \zeta \quad (34)$$

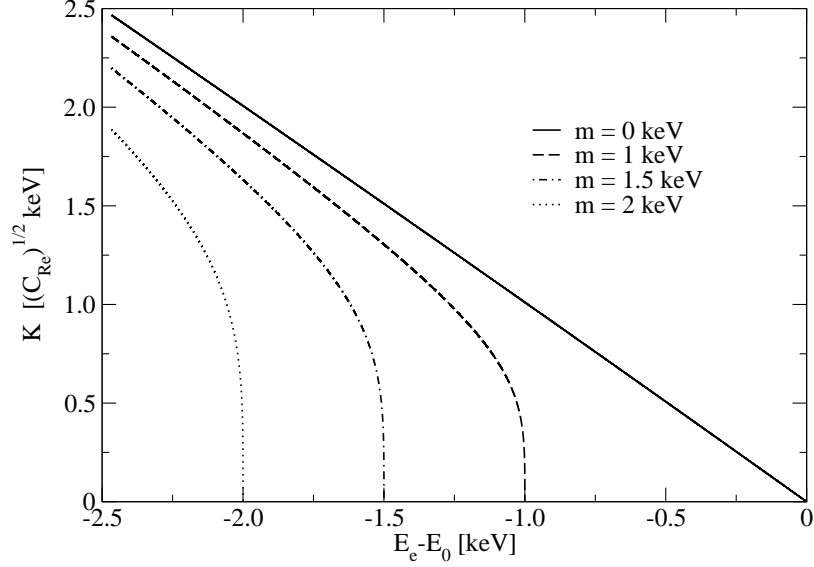


FIG. 7: Kurie plot K of the process ^{187}Re to ^{187}Os for different neutrino masses, $m = 0, 1, 1.5$ and 2 keV.

and

$$\frac{d\Gamma_{s1/2}^{\chi}}{dE_e} = CB_T p_e p_{\nu_{\chi}} E_e (E_0 - E_e) F_0(Z, E_e) \theta(E_0 - E_e - m_{\chi}) \quad , \quad \chi = l, s \quad , \quad (35)$$

as the shape factor $S(p_e, p_{\nu})$ is 1 for allowed decays. The relativistic Fermi function $F_0(Z, E_e)$ was defined in Eq. 13. The squared r.m.e. for the allowed decay of Tritium (T) is $B_T = B_{F_T} + B_{GT_T}$, where B_F and B_{GT} are the Fermi and Gamow-Teller decay strengths respectively, given by:

$$B_{F_T} = \frac{1}{2} |\langle {}^3\text{He}(1/2^+) \parallel \sum_{j=1}^{A=3} \tau_j^+ \parallel {}^3\text{H}(1/2^+) \rangle|^2 \quad (36)$$

and

$$B_{GT_T} = \frac{g_A^2}{2} |\langle {}^3\text{He}(1/2^+) \parallel \sum_{j=1}^{A=3} \tau_j^+ \vec{\sigma}_j \parallel {}^3\text{H}(1/2^+) \rangle|^2 \quad (37)$$

where $g_A = c_A/c_V \simeq 1.26$ is the axial-to-vector strength ratio of the charged weak interaction.

From the experimental mean-life of Tritium the decay strength can be obtained from

$$B_T^{-1} = \tau C \int_{m_e}^{E_0} p_e p_{\nu} E_e (E_0 - E_e) F_0(Z, E_e) dE_e \quad , \quad (38)$$

which yields a value $B_T \simeq 5.61$. In Fig. 8 we plot the differential decay rates of the process ${}^3\text{H}$ to ${}^3\text{He}$ for neutrinos of different masses. As an illustration of the heavy neutrino contribution to the total decay rate of the Tritium beta decay, we plot the electron spectrum in Fig. 9 with (solid line) and without (dashed line) sterile neutrino contribution with mass $m_s = 1$ keV and mixing angle 0.01° . The effect is made visible in the inset thanks to the indicated magnification. Finally, in Fig. 10 we plot the ratio \mathcal{R} vs. p_e for a fixed sterile neutrino mass ($m_s = 1$ keV) and different mixing angles.

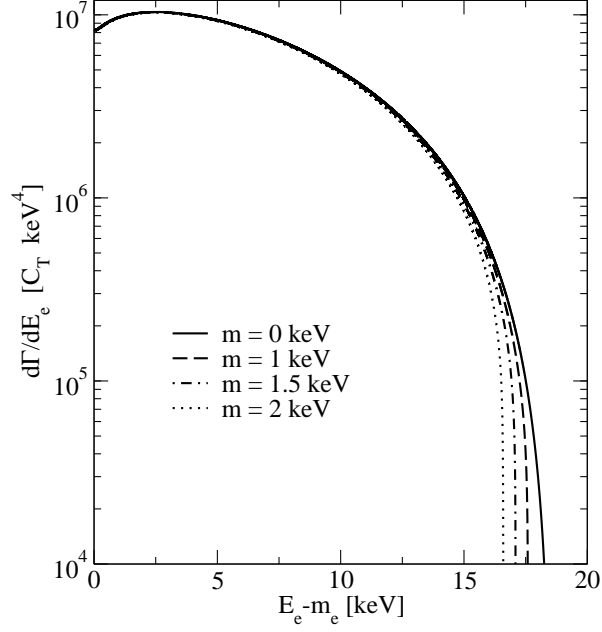


FIG. 8: Differential decay rate for the process ${}^3\text{H}$ going to ${}^3\text{He}$ with the emission of active ($m = 0$) or sterile ($m = 1, 1.5, 2$ keV) neutrinos, in units of $C_T \text{ keV}^4$. The vertical axis is in logarithmic scale.

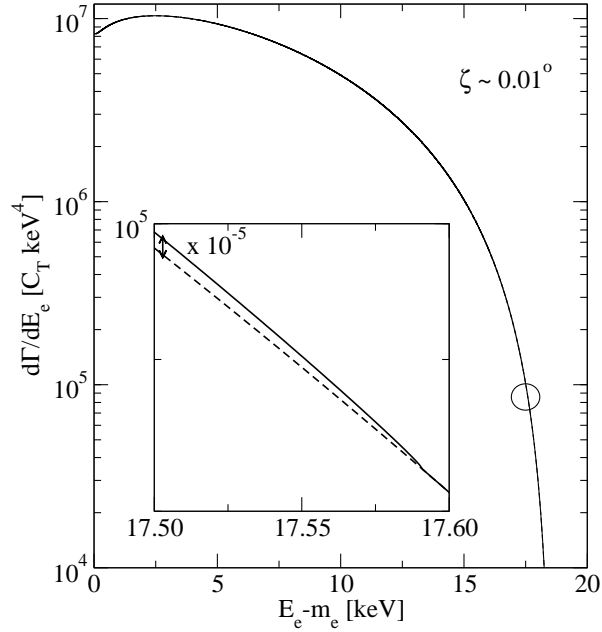


FIG. 9: The ${}^3\text{H}$ to ${}^3\text{He}$ beta particle spectrum with (solid line) and without (dashed line) sterile neutrino contribution for sterile mass $m_s = 1$ keV and $\zeta = 0.01^\circ$. Axis labels of the inset are the same as in the main plot, where a magnification of the separation between curves is magnified as indicated.

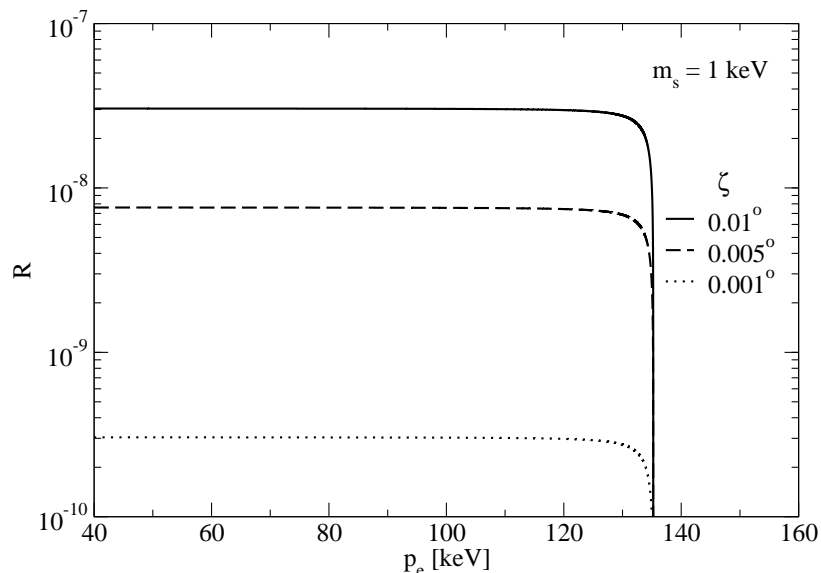


FIG. 10: Ratio \mathcal{R} , Eq. (17), vs. the electron momentum for a fixed sterile neutrino mass $m_s = 1$ keV and different mixing angles, for the process ${}^3\text{H}$ going to ${}^3\text{He}$.

VI. CONCLUSIONS

The detection of sterile neutrinos is not only important from the point of view of particle physics for the extension of the SM, but also from the point of view of cosmology and astrophysics as a serious candidate for dark matter in the keV mass range. With the relevance of the possible detection of keV scale dark matter candidates in mind, we have studied Rhenium 187 and Tritium beta decays. The low electron energy domain of the beta spectrum is the region where a sterile neutrino could be detected and its mass measured, the expected mass being in the keV scale (1 to 10 keV) as constrained from cosmological and galactic observations and theoretical analysis. The electron low energy region that is suitable to detect the sterile neutrino, $0 \lesssim T_e \lesssim (Q_\beta - m_s)$, is away from the endpoint energy region suitable for the detection of the active neutrino mass.

Two experiments are running at present, MARE and KATRIN, dealing with Rhenium 187 and Tritium beta decays respectively. The MARE experiment will provide the entire shape of the electron differential decay rate, giving data for both the sterile and the active neutrino detection regions. KATRIN so far concentrates on the region near the endpoint of the electron spectrum but it would be extremely interesting to look for data in the region where keV sterile neutrinos could show up [14]. In this paper, we have carried out the study of the role of sterile neutrinos in beta decay spectra, within the expected keV mass range and considering different mixing angles, according to astronomical and cosmological observations and experiments.

For ${}^{187}\text{Re}$ the electrons can be emitted in p -wave and in s -wave, the former dominating the decay by a factor 10^4 over the latter. For Tritium the electrons are emitted in s -wave only. The spectra of the electrons emitted in these waves have been carefully computed from the experimental beta decay half-lives using relativistic Fermi functions. Results for different neutrino masses (light and in the 1-2 keV range) have been obtained separately and mixed. We have also computed for both decays the ratio \mathcal{R} of the light to the heavy component of the mixing. It is different from zero in an electron momentum range $0 \leq p_e < (p_e)_{\text{max}}$, where $(p_e)_{\text{max}}$ decreases with increasing sterile neutrino mass m_s (equivalently for electron kinetic energy range). In the vicinity of $(p_e)_{\text{max}}$ the ratio \mathcal{R} drops off sharply, but in the rest of the range it exhibits an almost constant plateau with a slight increase as p_e goes to zero. It increases with the mixing angle and decreases with the sterile neutrino mass m_s .

In order to detect the small deviation in the experimental spectrum due to the sterile neutrino mixing, the relative experimental random error (inversely proportional to the square root of the number of measured events, $\epsilon \sim N_\beta^{-1/2}$) must be as small as possible. To this end, the number of detected events N_β must increase by choosing, for instance, a beta decay with a small Q_β value or by increasing the time of data acquisition. For MARE, the typical number of

events is $10^{13} - 10^{14}$ for 10 years of data acquisition, 8 arrays and 400 gr of natural Rhenium [9]. We found that at its largest value, the ratio \mathcal{R} of the sterile neutrino to the active neutrino contributions is about 10^{-8} using a realistic mixing angle. Therefore the sterile neutrino probability $\mathcal{R} \times N_\beta$ is about $10^5 - 10^6$, which is not negligible. It implies finding $10^5 - 10^6$ sterile neutrinos within $10^{13} - 10^{14}$ events. These numbers increase one order of magnitude for the MARE option of 10^{15} events for 10 years of data acquisition, 16 arrays and 3.2 kg of natural Rhenium [9]. A simple estimate requires the Poisson error ϵ to be smaller than the ratio \mathcal{R} . Namely, $N_\beta > 1/\mathcal{R}^2 \sim 10^{14} - 10^{15}$. Of course, in order to assess a precise prediction of the detection probability one should include a careful analysis of the systematic errors and instrument parameters, but such study goes beyond the scope of the present paper. The small effect expected on the electron spectrum calls for sources with larger stability to reduce the systematic errors, which pose at present a difficult challenge on the detection capabilities of these experiments. Furthermore, for $\mathcal{R} = 10^{-8}$ there would be one sterile neutrino event for one hundred million active neutrino events.

The main purpose of this paper has been to guide future experimental searches for sterile neutrinos. From the point of view of particle physics, one is talking about an extension of the Standard Model. From the point of view of cosmology, one is looking for a keV candidate for DM (mass range favoured by cosmological observations). Therefore, we show in this paper the relevant energy range where experimentalists should focus on as well as the order of magnitude of the expected signal, both in absolute terms and with respect to the background.

Acknowledgments

We are grateful to Peter Biermann, Angelo Nucciotti (MARE) and Christian Weinheimer (KATRIN) for useful discussions. O.M and E.M.G acknowledge the Spanish Ministry of Science and Education for partial financial support (FIS 2008-01301, FIS 2011-23565 and FPA 2010-17142). M.R.M. acknowledges the financial support of the Spanish Ministry of Science and Education (FIS 2008-01323), and the kind hospitality of the Observatoire de Paris.

-
- [1] J. R. Bond, A. S. Szalay, ApJ 274 (1983) 443. J R Bond, A S Szalay, M S Turner, Phys. Rev. Lett. 48 (1982) 1636.
 - [2] C. J. Hogan, J. J. Dalcanton, Phys. Rev. D 62 (2000) 063511. J. J. Dalcanton, C. J. Hogan, ApJ 561 (2000) 35.
 - [3] S. Dodelson, L. M. Widrow, Phys. Rev. Lett. 72 (1994) 17. X. Shi, G. M. Fuller, Phys. Rev. Lett. 82 (1999) 2832. K. Abazajian, G. M. Fuller, M. Patel, Phys. Rev. D 64 (2001) 023501; K. Abazajian, G. M. Fuller, Phys. Rev. D 66 (2002) 023526; G. M. Fuller *et al.*, Phys. Rev. D 68 (2003) 103002; K. Abazajian, Phys. Rev. D 73 (2006) 063506. P. L. Biermann, A. Kusenko, Phys. Rev. Lett. 96 (2006) 091301; T. Asaka, M. Shaposhnikov, A. Kusenko; Phys. Lett. B 638 (2006) 401. A. Kusenko, F. Takahashi, T. T. Yanagida, Phys. Lett. B 693, 144 (2010). K. Petraki, A. Kusenko, Phys. Rev. D77: 065014 (2008).
 - [4] H.J. de Vega and N. Sánchez, Mon. Not. R. Astron. Soc. 404 (2010) 885, astro-ph/0901.0922. D. Boyanovsky, H.J. de Vega and N. Sánchez, Phys. Rev. D 77 (2008) 043518.
 - [5] H.J. de Vega and N. Sánchez Int. J. Mod. Phys. A 26 (2011) 1057. H.J. de Vega, P. Salucci and N. Sánchez, New Astronomy, 17, 653 (2012).
 - [6] A. D. Dolgov, Phys. Rept. 370 (2002) 333. A. Kusenko, Phys. Rept. 481 (2009) 1.
 - [7] F. Munyaneza, P. L. Biermann, Astron. and Astrophys. 458 (2006) L9. D. Boyanovsky, C. M. Ho, JHEP (2007) 0707.
 - [8] F. D. Steffen, Eur. Phys. J. C 59 (2009) 557.
 - [9] MARE collaboration, <http://mare.dfm.uninsubria.it/frontend/exec.php>; A. Nucciotti, Neutrino 2010, arXiv:1012.2290. A. Nucciotti, on behalf of the MARE collaboration, *The MARE experiment and its capabilities to measure the light (active) and heavy (sterile) neutrinos*, lecture at the Chalonge Meudon Workshop 2011: Warm Dark Matter in the Galaxies, Theory and Observations, available at <http://chalonge.obspm.fr/>
 - [10] M. Galeazzi *et al.*, Phys. Rev. Lett. 86 (2001) 1978.
 - [11] R. Dvornický, K. Muto, F. Šimkovic and A. Faessler, Phys. Rev. C 83 (2011) 045502.
 - [12] C. Arnaboldi *et al.*, Phys. Rev. Lett. 96 (2006) 042503.
 - [13] KATRIN collaboration, <http://www-ik.fzk.de/tritium/>; C. Weinheimer, Varenna Enrico Fermi Course CLXX, arXiv:0912.1619. C. Weinheimer, 'Absolute Scale of the Neutrino Mass and the Search for Neutrinoless Double Beta Decay', lecture at the 15th Paris Cosmology Colloquium 2011: From CDM to WDM in the Standard Model of the Universe: Theory and Observations, available at <http://chalonge.obspm.fr/>
 - [14] C. Weinheimer, private communication.
 - [15] R. E. Shrock, Phys. Lett. B 96 (1980) 159. R. E. Shrock, Phys. Rev. D 24 (1981) 1232. R. E. Shrock, 'Implications of Neutrino Masses and Mixing for Weak Processes', AIP Conf. Proc. 72 (2008) 368.
 - [16] B. Pontecorvo, Rep. Prog. Phys. 11 (1947) 32. S. Cook *et al.*, Phys. Rev. D 46 (1992) R6. G. Finocchiaro, R. E. Shrock, Phys. Rev. D 46 (1992) R888.
 - [17] G. Finocchiaro and R R Shrock, Phys. Rev D46, R888 (1992). F. Bezrukov, M. Shaposhnikov, Phys. Rev. D 75 (2007) 053005. S. Ando, A. Kusenko Phys. Rev. D81, 113006 (2010).

- [18] W. Liao, Phys. Rev. D 82 (2010) 073001. Y. F. Li, Zhi-Zhong Xing, Phys. Lett. B 695 (2011) 205 and JCAP 1108 (2011) 006.
- [19] J. J. Simpson, Phys. Rev. Lett. 54 (1985) 1891.
- [20] F. E. Wietfeldt, E. B. Norman, Phys. Rep. 273 (1996) 149.
- [21] A. Franklin, Rev. Mod. Phys. 67 (1995) 457.
- [22] F. Zwicky, Helv. Phys. Acta 6 (1933) 124.
- [23] J. H. Oort, ApJ 91 (1940) 273. See S. van den Bergh, astro-ph/0005314 for a history of the research on dark matter.
- [24] E. W. Kolb, M. S. Turner, *The Early Universe*, Addison-Wesley (1990).
- [25] D. Boyanovsky, H.J. de Vega and N. Sánchez, Phys. Rev. D 78 (2008) 063546.
- [26] S. Dodelson, *Modern Cosmology*, Academic Press, London (2003).
- [27] J Kormendy, K C Freeman, IAU Symposium, Sydney, 220 (2004) 377, arXiv:astro-ph/0407321. M. Spano et al., MNRAS, 383 (2008) 297. G. Gentile et al., Nature, 461 (2009) 627. F. Donato et al., MNRAS 397 (2009) 1169.
- [28] Y. Hoffman *et al.*, ApJ 671 (2007) 1108.
- [29] J. Zavala *et al.*, ApJ 700 (2009) 1779. E. Papastergis *et al.*, ApJ 739 (2011) 38, arXiv:1106.0710.
- [30] R. E. Smith, K. Markovic, Phys. Rev. D84 (2011) 063507. K. Markovic *et al.*, JCAP 1101 (2011) 022.
- [31] A. Kamada, N. Yoshida, *keV-mass sterile neutrino dark matter and the structure of galactic halos*, lecture at the 15th Paris Cosmology Colloquium 2011: From CDM to WDM in the Standard Model of the Universe: Theory and Observations, available at <http://chalonge.obspm.fr/>
- [32] H.J. de Vega and N. Sánchez, *Highlights and Conclusions of the Chalonge Meudon Workshop 2010, Dark Matter in the Universe*, astro-ph/1007.2411. H.J. de Vega and N. Sánchez, *Highlights and Conclusions of the Chalonge Meudon Workshop 2011, Warm Dark Matter in the Galaxies*, astro-ph/1109.3187.
- [33] H.J. de Vega, M.C. Falvella and N. Sánchez, *Highlights and Conclusions of the Chalonge 14th Paris Colloquium: The Standard Model of the Universe: Theory and Observations*, astro-ph/1009.3494.
- [34] V. Tikhonov, S. Gottloeber, G. Yepes and Y. Hoffman, MNRAS 399 (2009) 1611.
- [35] K. Petraki, Phys. Rev. D77: 105004 (2008). J Wu, C-M Ho, D. Boyanovsky, Phys. Rev. D80, 103511 (2009). D. Boyanovsky, J Wu, Phys. Rev. D83: 043524 (2011).
- [36] M. Loewenstein, A. Kusenko, P. L. Biermann, ApJ 700 (2009) 426. M. Loewenstein, A. Kusenko, ApJ 714 (2010) 652.
- [37] M. Loewenstein, A. Kusenko, ApJ 751 (2012) 82.
- [38] G. G. Raffelt and Shun Zhou, Phys. Rev. D 83 (2011) 093014.
- [39] M. Viel et al. Phys. Rev. D 71 (2005) 63534.
- [40] A. Boyarsky, O. Ruchayskiy, M. Shaposhnikov, Ann. Rev. Nucl. Part. Sci. 59 (2009) 191. A. Boyarsky, J. Lesgourgues, O. Ruchayskiy, M. Viel, Phys. Rev. Lett. 102 (2009) 201304.
- [41] M. Doi, T. Kotani and E. Takasugi, Prog. Theor. Phys. (Supp.) 83 (1985) 1.
- [42] M. Doi and T. Kotani, Prog. Theor. Phys. 87 (1992) 1207.
- [43] Y. Chikashige, R. N. Mohapatra, R. D. Peccei, Phys. Lett. B 98 (1981) 265. J. Schechter, J.W.F. Valle, Phys. Rev. D 25 (1982) 774. R. R. Volkas, Prog. Part. Nucl. Phys. 48 (2002) 161. M. Shaposhnikov, I. Tkachev, Phys. Lett. B 639 (2006) 414. F. Bezrukov, H. Hettmansperger, M. Lindner, Phys.Rev. D 81 (2010) 085032. M. Lindner, A. Merle, and V. Niro, JCAP 1101 (2011) 034. A. Merle and V. Niro, JCAP 07 (2011) 023.
- [44] H. Behrens and W. Buhring, *Electron radial wave functions and nuclear beta decay*. Clarendon Press Oxford 1982.